Numer. Math. (2000) 86: 539–563
Digital Object Identifier (DOI) 10.1007/s002110000189

Numerische Mathematik

Error analysis for a potential problem on locally refined grids

T. Washio[1], **C.W. Oosterlee**[2]

[1] C&C Media Research Laboratories, NEC Cooperation, 1-1, Miyazaki 4-chome, Miyamae-ku, Kawasaki, Kanagawa 216-8555, Japan; e-mail: washio@ccm.cl.nec.co.jp
[2] GMD, Institute for Algorithms and Scientific Computing, 53754 Sankt Augustin, Germany; e-mail: oosterlee@gmd.de

Received June 25, 1998 / Revised version received July 14, 1999 /
Published online June 8, 2000 –

Summary. For the simulation of biomolecular systems in an aqueous solvent a continuum model is often used for the solvent. The accurate evaluation of the so-called solvation energy coming from the electrostatic interaction between the solute and the surrounding water molecules is the main issue in this paper. In these simulations, we deal with a potential problem with jumping coefficients and with a known boundary condition at infinity. One of the advanced ways to solve the problem is to use a multigrid method on locally refined grids around the solute molecule. In this paper, we focus on the error analysis of the numerical solution and the numerical solvation energy obtained on the locally refined grids. Based on a rigorous error analysis via a discrete approximation of the Greens function, we show how to construct the composite grid, to discretize the discontinuity of the diffusion coefficient and to interpolate the solutions at interfaces between the fine and coarse grids. The error analysis developed is confirmed by numerical experiments.

Mathematics Subject Classification (1991): 65N06, 65N15, 65N50, 65N55

1. Introduction

We perform error analysis for a potential problem arising from modeling biomolecular systems with aqueous solvent. One of the major effects mediated by the aqueous solvent is a screening of electrostatic interaction. A

Correspondence to: C.W. Oosterlee

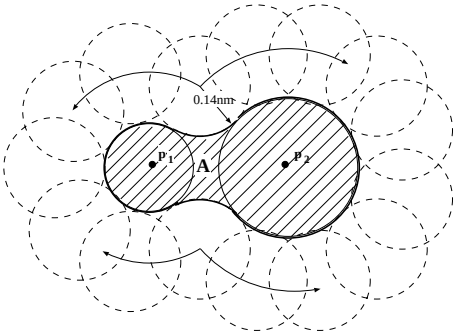

Fig. 1. The molecular surface (MS) is represented by the thick line curves. The Van der Waals surface is composed of the two surfaces of the atoms. A is the shaded volume which is enclosed by the MS

quantitative description of this screening can be formulated by a potential equation:

$$-\nabla \cdot (\epsilon(\mathbf{x})\nabla\psi_\epsilon(\mathbf{x})) = \sum_i q_i \delta_{\mathbf{p}_i}(\mathbf{x}), \tag{1}$$

where ϵ is the dielectric constant which depends on the position $\mathbf{x}$. The charge distribution in the solute molecule is represented by a set of point charges $\{q_i\delta_{\mathbf{p}_i}\}$ in the right hand side of (1). Usually, two ϵ regions are distinguished: the aqueous solvent has an ϵ-value of about 80 which models the orientational and electronic polarizability of water, whereas the solute molecule has an ϵ-value of about 1. Thus, we assume:

$$\epsilon(\mathbf{x}) = \begin{cases} \epsilon_0 \text{ for } \quad \mathbf{x} \in A \\ \epsilon_1 \text{ for } \mathbf{x} \in A^C \end{cases}, \tag{2}$$

where A is the open set corresponding to the solute molecule. The boundary of A is the so-called Molecular Surface[13] (MS) defined as the inward-facing surface generated by a sphere of radius 0.14 nm (the size of a water molecule) as it rolls over the Van der Waals surface of the solute molecule, which is the joint set of spheres with the Van der Waals radii. The volume enclosed by the MS ($= A$) is the volume from which water is excluded. From the definition of the MS, we can assume $\partial A \in C^1$. An example of a MS is depicted in Fig. 1, where the solute molecule is composed of 2 atoms. Since all the point charges $\{q_i\delta_{\mathbf{p}_i}\}$ are included in the solute molecule, we have:

$$\mathbf{p}_i \in A, \ \forall i. \tag{3}$$

One of the major interests in this area (for example see [8]) is the so called solvation energy defined by

$$W_S := \frac{1}{2}\int (\psi_\epsilon - \psi_{\epsilon_0})(\mathbf{x}) \left(\sum_i q_i \delta_{\mathbf{p}_i}(\mathbf{x}) \right) \, dx, \tag{4}$$

where ψ_{ϵ_0} is the potential in vacuum:

$$-\epsilon_0 \Delta \psi_{\epsilon_0}(\mathbf{x}) = \sum_i q_i \delta_{\mathbf{p}_i}(\mathbf{x}). \tag{5}$$

W_S is the difference in energy of the solute molecule in vacuum and in the solvent. Our goal is to find a fast and accurate way to compute the solvation energy confirmed by error analysis.

One of the important topics in this paper is the treatment of the Dirichlet boundary condition at infinity:

$$\psi_\epsilon(\mathbf{x}) \to 0 \text{ and } \psi_{\epsilon_0}(\mathbf{x}) \to 0 \text{ as } |\mathbf{x}| \to \infty \tag{6}$$

imposed on (1) and (5). A natural way to handle this boundary condition is by using locally refined grids around the solute molecule. Namely, we start with a fine grid around the solute molecule and construct a coarse grid with a larger domain size than the fine grid. We continue this process until we reach a satisfactorily large domain. Then, we impose a zero Dirichlet boundary value on the boundary of the coarsest grid. This technique is discussed in detail in Sect. 2, where we define a scalar value (the so-called grid extension rate) which characterizes the composite grid.

Another important topic is the treatment of the discontinuity of diffusion coefficient ϵ on ∂A in a finite volume discretization on a rectangular grid. In several papers dealing with jumping diffusion coefficients, for example in [1], [9] and [15], the discretization is given assuming that the jumps occur on grid points. However, since the MS is curved in our case, this can not be assumed here. We investigate the influence of a discretization of the ϵ-discontinuity on the accuracy of the numerical solutions in Sect. 3.2.

The discrete equations of (1) and (5) are solved on the composite grid, for example by the Multilevel Adaptive Technique (MLAT)[6] or by the Full Adaptive Composite (FAC)[12] method, in such a way that the discretization on the composite grid is guaranteed to be conservative. In this paper, we investigate a way to construct an optimal composite grid in the sense that the difference between the analytical and numerical solutions is reasonably small and the computational work is not too large. A similar topic is discussed in [3] and [4]. We also propose an interpolation method at the interfaces between the fine and coarse grids based on a conservative discretization of the diffusion term in (1). The proposed conservative interpolation results

in more accurate numerical solutions for our application than conventional interpolations like the cubic interpolation.

Based on the error analysis of the discrete Greens function in Sect. 3.2, we discuss the accuracy of the solvation energy in Sect. 3.3. The error estimate for this potential problem on a locally refined grid and the results obtained with this analysis are new. Based on this analysis, we obtain quantitative information about optimal grid coarsening towards infinity and on the size of the finest grid.

We summarize the notation used in this paper in Sect. 1.1 and introduce basic concepts to perform the error analysis.

1.1. Notation, definitions and basic concepts

Here, $\mathbf{x} = (x_1, x_2, x_3), \mathbf{y} = (y_1, y_2, y_3)$ are points in the three dimensional space.

- $|\mathbf{x}| := \max(|x_1|, |x_2|, |x_3|)$.
- $D_r(\mathbf{x}) := \{\mathbf{y} \in \mathbf{R^3} \ : \ |\mathbf{x} - \mathbf{y}| \leq r\}$.

- For any set A of points in the three dimensional space, we define

$$A^C := \{\mathbf{x} \in \mathbf{R^3} \ : \ \mathbf{x} \notin A\}.$$

- For a domain $B \subset \mathbf{R^3}$, $|B|$ stands for the volume of B.
- For a surface $S \subset \mathbf{R^3}$, $|S|$ stands for the surface area of S.
- $|f|_A :=$ the upper bound of $|f|$ on A (f is a function, $A \in \mathbf{R}^3$)
- For $A,\ B \subset \mathbf{R^3}$, $\mathrm{d}(A, B) := \min\{|\mathbf{x} - \mathbf{y}| \ : \ \mathbf{x} \in A,\ \mathbf{y} \in B\}$.

In this section, it will be shown that basic properties like Gauss's divergence theorem and Green's identity of analytical functions hold also on the discrete space with the discrete operators. These properties are frequently used in the error analysis in Sect. 3.

Let u be a discrete function on a uniform rectangular 3D grid with a grid spacing h. We can define a discrete flux $\nabla_h u$ at each center of a face connecting two neighboring grid points.

$$(\nabla_h u)_{i+1/2,j,k} := \frac{u_{i+1,j,k} - u_{i,j,k}}{h}, \quad \text{etc.} \tag{7}$$

Assume that a discrete diffusion coefficient $\widehat{\epsilon}$ defined on the central points of cell faces is given. Then, the diffusion operator associated with $\widehat{\epsilon}$ is given by

$$\begin{aligned} -\nabla_h \cdot (\widehat{\epsilon}\nabla_h u)_{i,j,k} := -\frac{1}{h^2}(&\widehat{\epsilon}_{i+1/2,j,k}(u_{i+1,j,k} - u_{i,j,k}) \\ &+\widehat{\epsilon}_{i,j+1/2,k}(u_{i,j+1,k} - u_{i,j,k}) \\ &+\widehat{\epsilon}_{i,j,k+1/2}(u_{i,j,k+1} - u_{i,j,k})). \end{aligned} \tag{8}$$

Let Ω be an arbitrary domain composed of finite volume cells. Then, we see that the following formula holds from Gauss's divergence theorem.

$$\int_{\Omega} \nabla_h \cdot (\widehat{\epsilon}(\mathbf{x})\nabla_h u(\mathbf{x}))\, dx = \oint_{\partial\Omega} \widehat{\epsilon}(\mathbf{s})\nabla_h u(\mathbf{s}) \cdot \vec{n}\, ds, \tag{9}$$

where $\vec{n}$ is the outward unit normal vector on $\partial\Omega$, and the integrands are regarded as step functions which are constant in each volume and on each cell face.

We can also prove Green's identity for any discrete functions u and v.

$$\begin{aligned} &\int_{\Omega} [u(\nabla_h \cdot (\widehat{\epsilon}\nabla_h v)) - (\nabla_h \cdot (\widehat{\epsilon}\nabla_h u))v]\, d\bar{x} \\ &= \oint_{\partial\Omega} \widehat{\epsilon}\,(u(\nabla_h v) - (\nabla_h u)v) \cdot \vec{n}\, ds. \end{aligned} \tag{10}$$

Note that u and v are not defined at the centers of cell faces. Therefore, the expression of the integrand in the right hand side of (10) is not precise. However, (10) holds if we define u and v at the center of each face by averaging two neighboring unknowns.

2. Discretization of the potential problem

In order to compute the solvation energy, we perform the following procedure. First, we solve two discrete equations,

$$-\nabla_h \cdot (\widehat{\epsilon}\nabla_h \psi_{\widehat{\epsilon},h}) = \sum_i q_i \delta_{\mathbf{p}_i,h}, \tag{11}$$

$$-\epsilon_0 \nabla_h \cdot (\nabla_h \psi_{\epsilon_0,h}) = \sum_i q_i \delta_{\mathbf{p}_i,h}, \tag{12}$$

of (1) and (5). Here, $\widehat{\epsilon}$ is ϵ_0 or ϵ_1 depending on the position in the grid. If a line segment intersects ∂A as shown in Fig. 2, $\widehat{\epsilon}$ is determined by the well-known weighted harmonic average [2]:

$$\widehat{\epsilon} = \epsilon_{har} := \frac{\epsilon_0\epsilon_1}{(1-\omega)\epsilon_0 + \omega\epsilon_1}. \tag{13}$$

Here, $(x + \omega h, y, z)$ is the intersection point between two adjacent grid points (x, y, z) and $(x + h, y, z)$. The basic idea of this discretization technique is similar to the idea of the Shortley-Weller discretization [10]. If $\widehat{\epsilon}$ is determined by (13), the following truncation error estimate is obtained by the Taylor expansion of ψ_ϵ at $(x + \omega h, y, z)$:

$$|(\widehat{\epsilon}(\mathbf{s})\nabla_h \psi_\epsilon(\mathbf{s}) - \epsilon(\mathbf{s})\nabla\psi_\epsilon(\mathbf{s})) \cdot \mathbf{e_1}| \le \widehat{\epsilon}\left|\nabla^2\psi_\epsilon\right|_{I(\mathbf{s}\setminus\partial A)} O(h). \tag{14}$$

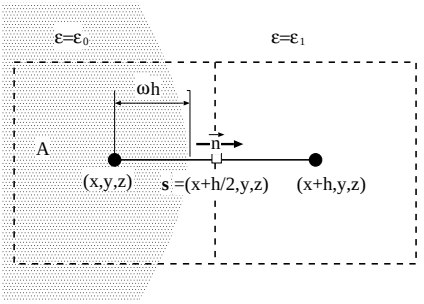

Fig. 2. Two grid points around ∂A. The broken lines represent the cell boundaries

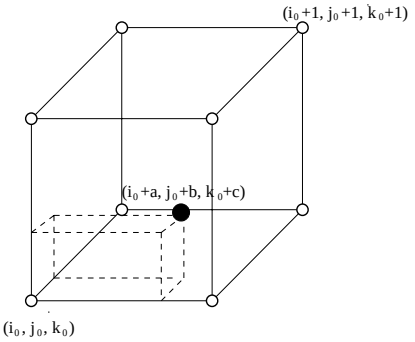

Fig. 3. The charge at • is distributed to the neighboring grid points ○

Here, $\mathbf{s} = (x+h/2, y, z)$, $\mathbf{e_1} = (1,0,0)$ and $I(\mathbf{s})$ is a line segment between (x,y,z) and $(x+h,y,z)$, which intersects ∂A (see Fig. 2). $|\nabla^2\psi_\epsilon|_{I(\mathbf{s})}$ is the upper-bound of $|\nabla^2\psi_\epsilon|$ on $I(\mathbf{s})$. Note that for the line segments that do not intersect ∂A, a smaller truncation error is obtained,

$$|(\widehat{\epsilon}(\mathbf{s})\nabla_h\psi_\epsilon(\mathbf{s}) - \epsilon(\mathbf{s})\nabla\psi_\epsilon(\mathbf{s}))\cdot\mathbf{e_1}| \le \widehat{\epsilon}\left|\nabla^3\psi_\epsilon\right|_{I(\mathbf{s})} O(h^2). \tag{15}$$

In the right hand side of (11) and (12), the discrete delta function $\delta_{\mathbf{p},h}$ for a given point $\mathbf{p}$ is obtained as follows. Point $\mathbf{p}$ included in a cube with vertices (i_0, j_0, k_0) and (i_0+1, j_0+1, k_0+1) corresponds to (i_0+a, j_0+b, k_0+c) in the space of the indices as depicted in Fig. 3. $\delta_{\mathbf{p},h}$ is now defined by

(16)

$$(\delta_{\mathbf{p},h})_{i,j,k} := \begin{cases} (1-a)(1-b) & \text{on} \quad (i,j,k) = (i_0, j_0, k_0), \\ \times(1-c)/h^3 & \\ a(1-b)(1-c)/h^3 & \text{on} \quad (i,j,k) = (i_0+1, j_0, k_0), \\ \cdots & \cdots, \\ abc/h^3 & \text{on} \quad (i,j,k) = (i_0+1, \\ & \quad j_0+1, k_0+1), \\ 0 & \text{otherwise.} \end{cases}$$

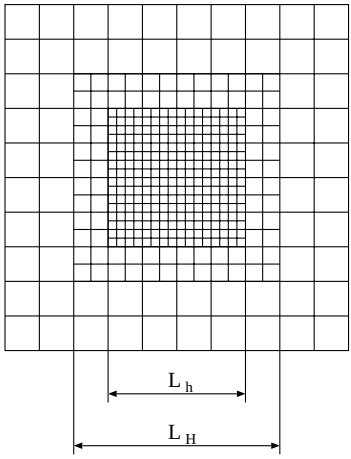

Fig. 4. The extended coarse grids around the finest grid

This distribution is necessary to obtain an $O(h^2)$ accurate numerical solution. From the solutions of (11) and (12), we compute an approximation of W_S in (4) by

$$W_{S,h} := \int (\psi_{\hat{\epsilon},h} - \psi_{\epsilon_0,h})(\mathbf{x}) \left(\sum_i q_i \delta_{\mathbf{p}_i,h}(\mathbf{x}) \right) dx. \tag{17}$$

2.1. Construction of extended coarse grids

In order to deal with the unbounded domain and with boundary condition (6), we start with a finest grid around the solute molecule and construct extended coarse grids around the finest grid, as shown in Fig. 4. We continue this process until a large enough domain size is reached, so that a zero boundary value can be imposed on the boundary of the coarsest grid. The ratio of the coarse grid domain size (L_H) to the fine grid domain size (L_h) is fixed in all of the extensions, see Fig. 4. We call this ratio the grid extension rate and denote it by α,

$$\alpha := \frac{L_H}{L_h} \ (\leq 2). \tag{18}$$

In this situation, the number of coarse grid points in one direction is approximately $\alpha n/2$ if the number of fine grid points along this direction is n. Hence, the number of grid points on the coarser grids tends to zero if we continue this process. We choose a grid extension rate of 2, once the grid size reaches a small number in the far field.

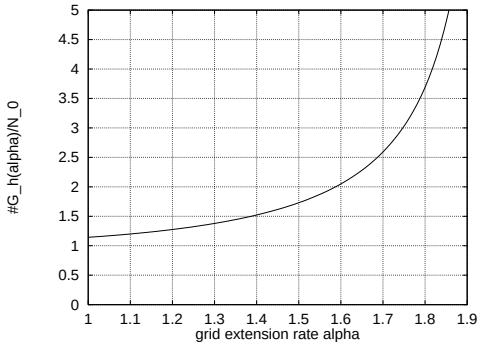

Fig. 5. The computational complexity with respect to the grid extension rate α

The grid extension rate α is an important factor for the accuracy of the solution and for the computational complexity. Since we adopt a multigrid V-cycle on the composite grid, the computational complexity is proportional to the sum of the grid points on all the levels, which is approximately estimated as

$$\sharp\mathcal{G}_h(\alpha) \approx N_0 + \left(\frac{\alpha}{2}\right)^3 N_0 + \left(\frac{\alpha}{2}\right)^{3\times 2} N_0 + \cdots = \frac{N_0}{1-\left(\frac{\alpha}{2}\right)^3}, \tag{19}$$

with N_0 the number of points on the finest grid. Here, $\mathcal{G}_h$ stands for the set of all grid points in the composite grid. In Fig. 5, the function $\frac{1}{1-\left(\frac{\alpha}{2}\right)^3}$ is depicted. It can be seen that the growth of the function is gentle up to $\alpha = 1.6$. However, it rapidly increases for $\alpha > 1.6$.

In Sect. 3, the best α in terms of both, the accuracy and the computational complexity is determined.

2.2. Conservative discretization and interpolation on interior boundaries

Here, we construct an interpolation technique on the interior boundary points of the composite grid based on a conservative finite volume discretization (see, for example, [7]) of the diffusion term $-\nabla\cdot(\epsilon\nabla\psi)$. The interpolation technique is explained for the 2D case. However, the technique is applied in 3D without any difficulty.

Figure 6 (a) shows some cells around interior boundary points of a composite grid. Except for the fine grid boundary points, all grid points are covered by standard square cells. At the fine grid boundary points, the cells are extended in such a way that they neighbor the coarse cells. We consider the finite volume discretization for the shaded cell $\Omega_{x,y}$ in Fig. 6 (a). For all standard cells, we apply a standard conservative discretization. For the

shaded cell, the fluxes per unit length at three faces ((w) west, (e) east and (n) north) are given by the standard discretization :

$$f_w = \epsilon_{x-h/2,y}(\psi_{x,y} - \psi_{x-h,y})/h, \text{, etc.} \tag{20}$$

In order to keep the compatibility of the flux at the interface between the fine and coarse grid cells, the flux f_s at the southern face is determined by $f_s = \frac{1}{2}(F_l + F_r)$, where F_l and F_r are the fluxes of the coarse grid cells computed by

$$F_l = \epsilon_{x-h,y-h}(\psi_{x-h,y} - \psi_{x-h,y-2h})/(2h),$$
$$F_r = \epsilon_{x+h,y-h}(\psi_{x+h,y} - \psi_{x+h,y-2h})/(2h).$$

Then the net flux of the shaded cell $\Omega_{x,y}$ is given by

$$\text{Flux}(\Omega_{x,y}) = (3/2)h(f_e - f_w) + h(f_n - f_s). \tag{21}$$

We now present an equivalent discretization, however, with Dirichlet boundary values on the interior boundary points, that are obtained by interpolation. This leads to a simple multilevel solution method on locally refined grids without losing the conservation property of the discretization on the composite grid. We only have to deal with simple stencils (5-point in 2D and 7-point in 3D) on a uniform mesh at each level with interpolated Dirichlet boundary values. Related formulations of the interpolation at the interior boundaries can be found in [5], [12] and [14]. An equivalent discretization is done in the following way. Figure 6 (b) shows the same situation as Fig. 6 (a).

In the situation presented in Fig. 6 (b), the net flux of standard cell $\tilde{\Omega}_{x,y}$ is given by

$$\text{Flux}(\tilde{\Omega}_{x,y}) = h(f_e - f_w) + h(f_n - \tilde{f}_s). \tag{22}$$

Here, the fluxes f_w, f_e and f_n are the same fluxes as the ones defined in (20). $\tilde{f}_s$ is defined by

$$\tilde{f}_s = \epsilon_{x,y-h/2}(\psi_{x,y} - \psi_{x,y-h})/h, \tag{23}$$

where $\psi_{x,y-h}$ is the Dirichlet boundary value on the grid point represented by $\circ$ at $(x, y-h)$ in Fig. 6 (b). In order to obtain identical discretizations in both situations in Fig. 6 (a) and (b), we equate the two net fluxes per unit volume (21) and (22):

$$\frac{\text{Flux}(\Omega_{x,y})}{3h^2/2} = \frac{\text{Flux}(\tilde{\Omega}_{x,y})}{h^2}. \tag{24}$$

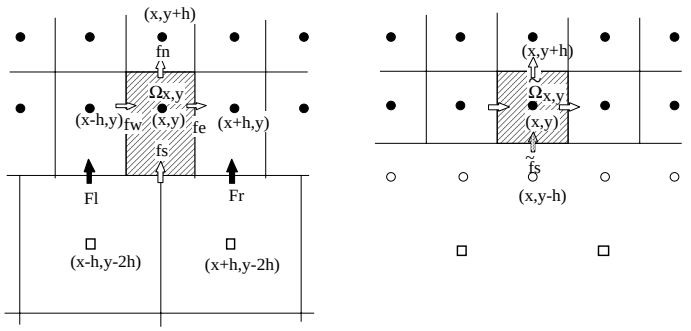

Fig. 6a,b. Two variants of a locally refined grid discretization with • fine grid points, □ coarse grid points which are not included in the fine grid, and ○ fine grid Dirichlet boundary points, where interpolation takes place. **a** A conservative discretization at the interior boundary points and **b** The situation with Dirichlet interior boundary points

From this equality, we obtain the interpolation formula for the flux $\tilde{f}_s$:

$$\tilde{f}_s = \frac{f_n + 2f_s}{3}. \tag{25}$$

Once the flux $\tilde{f}_s$ is obtained from (25), it is possible to compute the boundary value $\psi_{x,y-h}$ by solving (23),

$$\psi_{x,y-h} = \psi_{x,y} - \frac{\tilde{f}_s h}{\epsilon_{x,y-h/2}}. \tag{26}$$

When the diffusion coefficient ϵ is constant, the interpolation (26) results in a quadratic interpolation. Hence, the order of the interpolation ($O(h^3)$) is lower than the cubic interpolation ($O(h^4)$), which is frequently used for second order elliptic problems on locally refined grids. However, the numerical experiments in Sect. 4 confirm the superiority of the conservative interpolation over the cubic interpolation even in the case of $\epsilon \equiv 1$ at the interior boundaries in our applications with many refinement levels. In Sect. 3.2, we also see that the conservative interpolation is sufficient to properly bound the error.

In preparation for the error analysis in Sect. 3.2, we estimate the truncation error of the conservative discretization at the interior boundaries. Assume (x, y) is a fine grid cell center at level l, which neighbors a coarse grid cell at $(x, y - h_l)$. Here, h_l is the grid spacing at the level l. Let ψ be an arbitrary C^3 function. Since all cell faces are located at the centers of two adjacent grid points, we obtain the following estimates of the truncation

error at cell faces of $\Omega_{x,y}$

$$\left|\nabla_h\psi(x-h_l/2,y)-\frac{\partial\psi}{\partial x}(x-h_l/2,y)\right| \leq \left|\frac{\partial^3\psi}{\partial x^3}\right|_{([x-h_l,x],y)} O({h_l}^2), \tag{27}$$

$$\left|\nabla_h\psi(x+h_l/2,y)-\frac{\partial\psi}{\partial x}(x+h_l/2,y)\right| \leq \left|\frac{\partial^3\psi}{\partial x^3}\right|_{([x,x+h_l],y)} O({h_l}^2), \tag{28}$$

$$\left|\nabla_h\psi(x,y-h_l)-\frac{\partial\psi}{\partial y}(x,y-h_l)\right| \leq \left|\frac{\partial^3\psi}{\partial y^3}\right|_{(x,[y-2h_l,y])} O({h_l}^2), \tag{29}$$

$$\left|\nabla_h\psi(x,y+h_l/2)-\frac{\partial\psi}{\partial y}(x,y+h_l/2)\right| \leq \left|\frac{\partial^3\psi}{\partial y^3}\right|_{(x,[y,y+h_l])} O({h_l}^2). \tag{30}$$

An inequality similar to (30) holds even if $(x, y-h_l)$ is located at an intersection of two coarse grid cell faces as in Fig. 6 (a). This follows from Taylor's expansion

$$\left|\frac{1}{2}\left(\frac{\partial\psi}{\partial y}(x-h_l,y-h_l)+\frac{\partial\psi}{\partial y}(x+h,y-h_l)\right)-\frac{\partial\psi}{\partial y}(x,y-h_l)\right| \leq \left|\frac{\partial^3\psi}{\partial x^2\partial y}\right|_{([x-h_l,x+h],y-h_l)} O({h_l}^2), \tag{31}$$

and with the definition of $\nabla_h\psi$ at $(x, y-h_l)$:

$$\nabla_h\psi(x,y-h_l)=\frac{1}{2}(\nabla_h\psi(x-h_l,y-h_l)+\nabla_h\psi(x+h_l,y-h_l)). \tag{32}$$

From the Taylor expansion of $\frac{\partial \psi}{\partial x}$ and $\frac{\partial \psi}{\partial y}$ at (x, y), we then find

$$\left| \frac{\partial^2 \psi}{\partial x^2}(x,y) - \frac{1}{h_l}\left(\frac{\partial \psi}{\partial x}(x + h_l/2, y) - \frac{\partial \psi}{\partial x}(x - h_l/2, y) \right) \right|$$

$$\leq \left| \frac{\partial^3 \psi}{\partial x^3} \right|_{([x-h_l/2, x+h_l/2], y)} O(h_l), \tag{33}$$

$$\left| \frac{\partial^2 \psi}{\partial y^2}(x,y) - \frac{2}{3h_l}\left(\frac{\partial \psi}{\partial y}(y + h_l/2, y) - \frac{\partial \psi}{\partial y}(x - h_l, y) \right) \right|$$

$$\leq \left| \frac{\partial^3 \psi}{\partial y^3} \right|_{(x, [y-h_l, y+h_l/2])} O(h_l). \tag{34}$$

From (27–30), (33) and (34), we obtain the following estimate at the interior boundaries

$$|\Delta\psi(x,y) - \nabla_h \cdot \nabla_h \psi(x,y)| \leq |\nabla^3 \psi|_{[x-h_l, x+h_l]\times[y-2h_l, y+h_l]} O(h_l). \tag{35}$$

Note that, for the grid points, that are located at the cell center, a better upper bound can be found as

$$|\Delta\psi(x,y) - \nabla_h \cdot \nabla_h \psi(x,y)| \leq |\nabla^4 \psi|_{[x-h_l, x+h_l]\times[y-h_l, y+h_l]} O({h_l}^2). \tag{36}$$

Equation (36) holds also at the interior boundaries if we define $\nabla_h \cdot \nabla_h$ based on cubic interpolation. However, we will see in the numerical experiments in Sect. 4 that the conservative interpolation proposed provides a much better accuracy than cubic interpolation.

3. Error analysis

In this section the error of the numerical solvation energy in (17) is estimated. The size of the error depends on several important choices: the grid extension rate from Sect. 2.1, the interpolation method at the interior boundaries in Sect. 2.2 and the discretization at the discontinuity in ϵ. We start with the error analysis of the Green function inside the finest grid in Sect. 3.2. In Sect. 3.3, we estimate the error of the numerical solvation energy based on the results obtained in Sect. 3.2.

3.1. Definition of Green functions

Let $G(\mathbf{y}, \mathbf{p})$ be the Green function for the operator $-\nabla \cdot (\epsilon \nabla\ )$,

$$-\nabla \cdot (\epsilon(\mathbf{y}) \nabla G(\mathbf{y}, \mathbf{p})) = \delta_{\mathbf{p}}(\mathbf{y}) \text{ for } \mathbf{y}, \mathbf{p} \in \mathbf{R^3}. \tag{37}$$

Here, ∇ acts on variable $\mathbf{y}$. Let $b(A)$ be the set of cells, whose central grid point $\mathbf{y}$ satisfies

$$\mathrm{d}(\mathbf{y}, \partial A) \leq h_0, \tag{38}$$

with h_0 the grid spacing on the finest grid. As in the case $\epsilon \equiv \epsilon_0$ [11], let there be given constants $c_k (k = 0, 1, 2, \cdots)$ such that

$$|\nabla_y{}^{k-m} \nabla_p{}^m G(\mathbf{y}, \mathbf{p})| \leq \frac{c_k}{|\mathbf{y} - \mathbf{p}|^{k+1}}, \ (m \leq k) \text{ for } \mathbf{y}, \mathbf{p} \notin \partial A. \tag{39}$$

Here, ∇_y and ∇_p act on variables $\mathbf{y}$ and $\mathbf{p}$, respectively. Let $\mathcal{G}_h$ be the set of all grid points of the composite grid. For given $\mathbf{y} \in \mathbf{R^3}$ and $\mathbf{p} \in \mathcal{G}_h$, we define the cell averaged Green function $\widetilde{G}(\mathbf{y}, \mathbf{p})$ by

$$\widetilde{G}(\mathbf{y}, \mathbf{p}) := \frac{1}{|\Omega_p|} \int_{\Omega_p} G(\mathbf{y}, \mathbf{z}) \, dz. \tag{40}$$

Here, Ω_p represents the cell, which includes grid point $\mathbf{p}$, $|\Omega_p|$ is its volume.

Let D_l $(l = 0, 1, 2...)$ be the domain composed of the cubic cells of grid $\mathcal{G}_l$ at level l and $b(D_l)$ be the set of non-cubic cells (Fig. 6 (a)) covering the boundary grid points of $\mathcal{G}_l$.

From (39), we can also assume

$$|\nabla_y{}^k \widetilde{G}(\mathbf{y}, \mathbf{p})| \leq \frac{c_k}{|\mathbf{y} - \mathbf{p}|^{k+1}}, \text{ for } \mathbf{y}, \mathbf{p} \notin b(A). \tag{41}$$

For a given grid point $\mathbf{y} \in \mathcal{G}_h$, $h(\mathbf{y})$ is the grid spacing at $\mathbf{y}$,

$$h(\mathbf{y}) = 2^l h_0 \text{ if } \mathbf{y} \in \mathcal{G}_l \text{ and } \mathbf{y} \notin \mathcal{G}_{l-1}. \tag{42}$$

Let G_h be the discrete Green function of the discrete operator $-\nabla_h \cdot (\widehat{\epsilon} \, \nabla_h \ )$ on the composite grid,

$$-\nabla_h \cdot (\widehat{\epsilon}(\mathbf{y}) \nabla_h G_h(\mathbf{y}, \mathbf{p})) = \delta_{\mathbf{p},h}(\mathbf{y}). \tag{43}$$

Here, $\nabla_h \cdot$ and ∇_h act on variable $\mathbf{y}$, and $\delta_{\mathbf{p},h}$ is the discrete delta function defined in (16).

If we apply the conservative discretization at the interior boundaries as explained in Sect. 2.2, Green's identity (10) holds for discrete functions on $\mathcal{G}_h$. Hence, we have

$$\begin{aligned} &\int_{D_l} G_h(\mathbf{x}, \mathbf{y})[-\nabla_h \cdot (\widehat{\epsilon}(\mathbf{y}) \nabla_h \psi_h(\mathbf{y}))] \, dy \\ &\quad = \psi_h(\mathbf{x}) - \oint_{\partial D_l} \widehat{\epsilon}(\mathbf{s})[G_h(\mathbf{x}, \mathbf{s})(\nabla_h \psi_h(\mathbf{s})) \\ &\qquad -(\nabla_h G_h(\mathbf{x}, \mathbf{s}))\psi_h(\mathbf{s})] \cdot \vec{n} \, ds \end{aligned} \tag{44}$$

for any discrete function ψ_h and $l \geq 0$. In particular, if we assume the following asymptotic behavior of the discrete functions:

$$|G_h(\mathbf{x},\mathbf{y})| \leq \frac{\bar{c}}{|\mathbf{x}-\mathbf{y}|},\ |\nabla_h G_h(\mathbf{x},\mathbf{y})| \leq \frac{\bar{c}}{|\mathbf{x}-\mathbf{y}|^2}, \tag{45}$$

$$|\psi_h(\mathbf{y})| \leq O\left(\frac{1}{|\mathbf{y}|}\right),\ |\nabla_h \psi_h(\mathbf{y})| \leq O\left(\frac{1}{|\mathbf{y}|^2}\right), \tag{46}$$

we obtain

$$\lim_{l\to\infty} \oint_{\partial D_l} \widehat{\epsilon}(\mathbf{s})[G_h(\mathbf{x},\mathbf{s})(\nabla_h \psi_h(\mathbf{s})) - (\nabla_h G_h(\mathbf{x},\mathbf{s}))\psi_h(\mathbf{s})] \cdot \vec{n}\ ds = 0.$$

Therefore, the following formula holds as in the analytic case.

$$\int G_h(\mathbf{x},\mathbf{y})[-\nabla_h \cdot (\widehat{\epsilon}(\mathbf{y})\nabla_h \psi_h(\mathbf{y}))]\ dy = \psi_h(\mathbf{x}). \tag{47}$$

3.2. Error estimate of Green functions on the finest grid

In this section, we estimate the difference between $\widetilde{G}(\mathbf{x},\mathbf{p})$ and $G_h(\mathbf{x},\mathbf{p})$. From (43) and (47), the difference can be represented by

$$\begin{aligned} e(\mathbf{x},\mathbf{p}) &:= \widetilde{G}(\mathbf{x},\mathbf{p}) - G_h(\mathbf{x},\mathbf{p}) \\ &= \int G_h(\mathbf{x},\mathbf{y})\{-\nabla_h \cdot [\widehat{\epsilon}(\mathbf{y})\nabla_h(\widetilde{G}(\mathbf{y},\mathbf{p}) - G_h(\mathbf{y},\mathbf{p}))]\}\ dy \\ &= \int G_h(\mathbf{x},\mathbf{y})[-\nabla_h \cdot (\widehat{\epsilon}(\mathbf{y})\nabla_h \widetilde{G}(\mathbf{y},\mathbf{p})) - \delta_{\mathbf{p},h}(\mathbf{y})]\ dy. \end{aligned} \tag{48}$$

In order to also estimate the difference of the finite differences $\nabla_h \widetilde{G}(\mathbf{x},\mathbf{p})$ and $\nabla_h G_h(\mathbf{x},\mathbf{p})$ with respect to variable $\mathbf{x}$, we estimate the quantity $e(\mathbf{x},\mathbf{p};\delta\mathbf{x})$ for a small displacement $\delta\mathbf{x}$,

$$\begin{aligned} e(\mathbf{x},\mathbf{p};\delta\mathbf{x}) &:= e(\mathbf{x}+\delta\mathbf{x},\mathbf{p}) - e(\mathbf{x},\mathbf{p}) \\ &= \int (G_h(\mathbf{x}+\delta\mathbf{x},\mathbf{y}) - G_h(\mathbf{x},\mathbf{y}))\left(-\nabla_h \cdot (\widehat{\epsilon}(\mathbf{y})\nabla_h \widetilde{G}(\mathbf{y},\mathbf{p}))\right. \\ &\quad \left. - \delta_{\mathbf{p},h}(\mathbf{y})\right)\ dy. \end{aligned} \tag{49}$$

The estimate of the error in $\nabla_h G_h$ is necessary for the error analysis of the solvation energy in Sect. 3.3. We estimate these errors under the following conditions (depicted in Fig. 7).

$$\begin{cases} A \subset D_0, \\ \mathbf{x},\mathbf{p} \in A \text{ and } \mathbf{x},\mathbf{p} \notin b(A)\ (\mathbf{x} \neq \mathbf{p}). \end{cases} \tag{50}$$

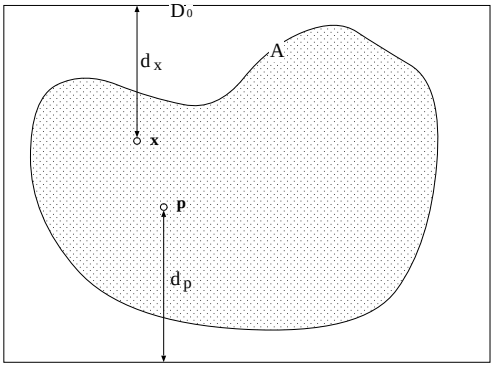

Fig. 7. Two points $\mathbf{x}$, $\mathbf{p}$ in A

Since our interests are the influences on the errors of the configuration of the composite grid and the discretization at the discontinuity of ϵ, we only estimate the partial integrals of (48) and (49) over the following regions:

$R_1 := {D_0}^C \cap (\overset{\infty}{\underset{l\geq 0}{\cup}} b(D_l))^C$: Outside the finest grid excluding the interior boundaries.

$R_2 := \overset{\infty}{\underset{l\geq 0}{\cup}} b(D_l)$: The non-cubic cells on the interior boundaries as in Fig. 6 (a).

$R_3 := b(A)$: The cells around ∂A

In the following, we represent the partial integrals on R_i by e_i. Regarding the relation between the errors and the composite grid configuration, the following theorem holds.

Theorem 3.1. *Let α be the grid extension rate of the composite grid (18), $|D_0|$ and $|\partial D_0|$ be the volume and the surface area of the finest grid domain D_0, respectively, and h_0 be the grid spacing on the finest grid. Let us assume that (45) holds. Then the partial integrals e_1 and e_2 are bounded as follows.*

$$|e_1(\mathbf{x},\mathbf{p})| \leq c\frac{\alpha^3-1}{1-2^2/\alpha^3}\frac{|D_0|{h_0}^2}{d_x{d_p}^5} \quad \text{if } \alpha > 2^{2/3}, \tag{51}$$

$$|e_1(\mathbf{x},\mathbf{p}:\delta\mathbf{x})| \leq c\frac{\alpha^3-1}{1-2^2/\alpha^4}\frac{|\delta\mathbf{x}||D_0|{h_0}^2}{{d_x}^2{d_p}^5} \text{ if } \alpha > 2^{1/2}, \tag{52}$$

$$|e_2(\mathbf{x},\mathbf{p})| \leq c\frac{1}{1-2^2/\alpha^3}\frac{|\partial D_0|{h_0}^2}{d_x{d_p}^4} \text{ if } \alpha > 2^{2/3}, \tag{53}$$

$$|e_2(\mathbf{x},\mathbf{p}:\delta\mathbf{x})| \leq c\frac{1}{1-2^2/\alpha^4}\frac{|\delta\mathbf{x}||\partial D_0|{h_0}^2}{{d_x}^2{d_p}^4} \quad \text{if } \alpha > 2^{1/2}. \tag{54}$$

Here, c is a constant depending only on some of the variables $c_k (k = 0, 1, 2, \dots)$ in (41), $\bar{c}$ in (45) and on the diffusion coefficient ϵ_1. d_x and d_p are the distances, respectively, from $\mathbf{x}$ and $\mathbf{p}$ to the boundary of the finest grid defined by $d_x := \mathrm{d}(\mathbf{x}, \partial D_0)$, $d_p := \mathrm{d}(\mathbf{p}, \partial D_0)$.

Proof. First, we estimate $|e_1|$. From (36) and (41) with $k = 4$, we obtain

(55)
$$\left|\nabla_h \cdot \nabla_h \widetilde{G}(\mathbf{y}, \mathbf{p})\right| \leq c \frac{h(\mathbf{y})^2}{|\mathbf{y} - \mathbf{p}|^5}, \text{ for } \mathbf{y} \in R_1 = {D_0}^C \cap (\overset{\infty}{\underset{l \geq 0}{\cup}} b(D_l))^C.$$

From (45) and (55), we obtain

$$|e_1(\mathbf{x}, \mathbf{p})| = \left| \int_{R_1} G_h(\mathbf{x}, \mathbf{y}) \epsilon_1 \nabla_h \cdot \nabla_h \widetilde{G}(\mathbf{y}, \mathbf{p}) \, dy \right|$$

(56)
$$\leq c \int_{{D_0}^C} \frac{h(\mathbf{y})^2}{|\mathbf{y} - \mathbf{x}||\mathbf{y} - \mathbf{p}|^5} \, dy.$$

Regarding $e_1(\mathbf{x}, \mathbf{p} : \delta\mathbf{x})$: from (45), we obtain

(57)
$$|G_h(\mathbf{x} + \delta\mathbf{x}, \mathbf{y}) - G_h(\mathbf{x}, \mathbf{y})| \leq c \frac{|\delta\mathbf{x}|}{|\mathbf{y} - \mathbf{x}|^2}.$$

Hence, we find the following upper bound

$$|e_1(\mathbf{x}, \mathbf{p} : \delta\mathbf{x})| = \left| \int_{R_1} (G_h(\mathbf{x}, \mathbf{y}) - G_h(\mathbf{x} + \delta\mathbf{x}, \mathbf{y})) \epsilon_1 \nabla_h \cdot \nabla_h \widetilde{G}(\mathbf{y}, \mathbf{p}) \, dy \right|$$

(58)
$$\leq c|\delta\mathbf{x}| \int_{{D_0}^C} \frac{h(\mathbf{y})^2}{|\mathbf{y} - \mathbf{x}|^2 |\mathbf{y} - \mathbf{p}|^5} \, dy.$$

From the definitions of d_x and d_p, and from the way in which the coarse grids are defined in Sect. 2.1, the following conditions are fulfilled

(59)
$$h(\mathbf{y}) = 2^l h_0 \text{ for } \mathbf{y} \in D_l \cap D_{l-1}^C,$$

(60)
$$|\mathbf{y} - \mathbf{x}| \geq \alpha^{l-1} d_x, \ |\mathbf{y} - \mathbf{p}| \geq \alpha^{l-1} d_p \text{ for } \mathbf{y} \in D_l \cap D_{l-1}^C,$$

(61)
$$|D_l \cap {D_{l-1}}^C| = (\alpha^{3l} - \alpha^{3(l-1)})|D_0|,$$

where $|D_l \cap {D_{l-1}}^C|$ and $|D_0|$ stand for the volumes of $D_l \cap {D_{l-1}}^C$ and D_0, respectively.
From (59), (60) and (61), we obtain

$$\int_{D_l \cap {D_{l-1}}^C} \frac{h(\mathbf{y})^2}{|\mathbf{y} - \mathbf{x}|^k |\mathbf{y} - \mathbf{p}|^5} \, dy \leq \frac{(2^l h_0)^2}{(\alpha^{l-1} d_x)^k (\alpha^{l-1} d_p)^5} \times (\alpha^{3l} - \alpha^{3(l-1)})|D_0|$$

(62)
$$= \frac{4 {h_0}^2 |D_0| (\alpha^3 - 1)}{{d_x}^k {d_p}^5} \left(\frac{2^2}{\alpha^{2+k}} \right)^{l-1}.$$

From (56) and (62) with $k = 1$, finally, we find the upper-bound of $|e_1(\mathbf{x}, \mathbf{p})|$:

$$|e_1(\mathbf{x}, \mathbf{p})| \leq c\frac{{h_0}^2|D_0|(\alpha^3 - 1)}{d_x {d_p}^5} \sum_{l=1}^{\infty} \left(\frac{2^2}{\alpha^3}\right)^{l-1}.$$

Regarding $|e_1(\mathbf{x}, \mathbf{p} : \delta\mathbf{x})|$: from (58) and (62) with $k = 2$, it can be bounded as

$$|e_1(\mathbf{x}, \mathbf{p} : \delta\mathbf{x})| \leq c\frac{|\delta\mathbf{x}|{h_0}^2|D_0|(\alpha^3 - 1)}{{d_x}^2 {d_p}^5} \sum_{l=1}^{\infty} \left(\frac{2^2}{\alpha^4}\right)^{l-1}.$$

The integrals over the interior boundary cells R_2 can be estimated similarly to the estimate for R_1. From (35) and (41) with $k = 3$, we obtain

$$\left|\nabla_h \cdot \nabla_h \widetilde{G}(\mathbf{y}, \mathbf{p})\right| \leq c\frac{h(\mathbf{y})}{|\mathbf{y} - \mathbf{p}|^4} \text{ for } \mathbf{y} \in R_2. \tag{63}$$

Hence, $|e_2(\mathbf{x}, \mathbf{p})|$ and $|e_2(\mathbf{x}, \mathbf{p}, \delta\mathbf{x})|$ can be bounded as follows

$$|e_2(\mathbf{x}, \mathbf{p})| \leq c \int_{R_2} \frac{h(\mathbf{y})}{|\mathbf{y} - \mathbf{x}||\mathbf{y} - \mathbf{p}|^4}\, dy, \tag{64}$$

$$|e_2(\mathbf{x}, \mathbf{p}, \delta\mathbf{x})| \leq c|\delta\mathbf{x}| \int_{R_2} \frac{h(\mathbf{y})}{|\mathbf{y} - \mathbf{x}|^2|\mathbf{y} - \mathbf{p}|^4}\, dy. \tag{65}$$

From (59) and (60) and the fact:

$$|b(D_l)| \leq 2^{l+1}h_0|\partial D_l| \approx 2^{l+1}h_0\alpha^{2l}|\partial D_0| \tag{66}$$

with $|\partial D_l|$ the area of ∂D_l, we obtain

$$\int_{b(D_l)} \frac{h(\mathbf{y})}{|\mathbf{y} - \mathbf{x}|^k|\mathbf{y} - \mathbf{p}|^4}\, dy \leq \frac{2^{l+1}h_0}{(\alpha^l d_x)^k(\alpha^l d_p)^4} 2^{l+1}h_0\alpha^{2l}|\partial D_0|$$

$$= \frac{4{h_0}^2|\partial D_0|}{{d_x}^k {d_p}^4} \left(\frac{2^2}{\alpha^{2+k}}\right)^l. \tag{67}$$

From (64), (65) and (67), we find the upper bounds of $|e_2|$. □

For the relation between the errors and the discretization of the discontinuity of ϵ, the following theorem holds.

Theorem 3.2. *Let us assume that the weighted harmonic averaging (13) is applied to determine $\widehat{\epsilon}$ and (45) holds. Then the partial integrals e_3 around the discontinuity are bounded as follows:*

$$|e_3(\mathbf{x}, \mathbf{p})| \leq cS^2(\partial A, \mathbf{p}){h_0}^2 \left(\frac{1}{a_x {a_p}^2} + \frac{1}{{a_x}^2 a_p}\right), \tag{68}$$

$$|e_3(\mathbf{x}, \mathbf{p} : \delta\mathbf{x})| \leq cS^2(\partial A, \mathbf{p})|\delta\mathbf{x}|{h_0}^2 \left(\frac{1}{{a_x}^2 {a_p}^2} + \frac{1}{{a_x}^3 a_p}\right). \tag{69}$$

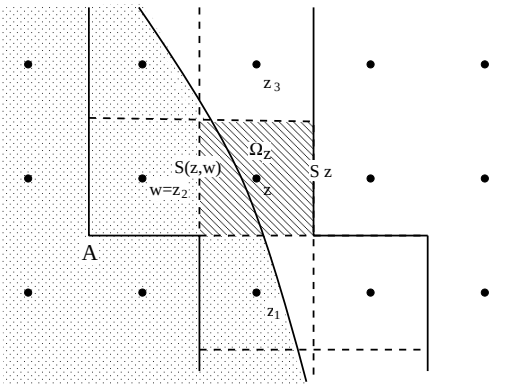

Fig. 8. A two dimensional image of $b(A)$. The area surrounded by the thick solid lines is $b(A)$. The broken lines represent the cell faces shared by two cells in $b(A)$

Here, c is a constant depending only on some of the variables $c_k (k = 0, 1, 2, \dots)$ in (41), $\bar{c}$ in (45) and ϵ_i $(i = 0, 1)$. a_x and a_p are distances, respectively, from $\mathbf{x}$ and $\mathbf{p}$ to the boundary of A defined by $a_x := \mathrm{d}(\mathbf{x}, \partial A)$, $a_p := \mathrm{d}(\mathbf{p}, \partial A)$. $S^2(\partial A, \mathbf{p})$ is defined by

$$S^2(\partial A, \mathbf{p}) := \oint_{\partial A} \frac{1}{|\mathbf{s} - \mathbf{p}|^2} ds. \tag{70}$$

Proof. In order to obtain an optimal upper bound for $|e_3|$, the cancellation of truncation errors of $-\nabla_h \cdot (\widehat{\epsilon} \nabla_h \widetilde{G}(\mathbf{y}, \mathbf{p}))$ between neighboring cells must be exploited. This is done by showing the cancellation of the error on a cell face shared by two neighboring cells in $b(A)$ after the application of Gauss's divergence theorem.

For any grid point $\mathbf{z} \in b(A)$, let $\mathbf{z}_i$ $(i = 1, 2, \cdots)$ be the grid points in $b(A)$, that share a cell face with $\mathbf{z}$ as depicted in Fig. 8.

From

$$\nabla \cdot (\epsilon(\mathbf{y}) \nabla \widetilde{G}(\mathbf{y}, \mathbf{p})) = 0 \text{ for } \mathbf{y} \in b(A)$$

and Gauss's divergence theorem (9), we obtain the following equality for a cell $\Omega_z \subset b(A)$.

$$\begin{aligned}
&\int_{\Omega_z} G_h(\mathbf{x}, \mathbf{y}) \nabla_h \cdot (\widehat{\epsilon}(\mathbf{y}) \nabla_h \widetilde{G}(\mathbf{y}, \mathbf{p}))\, dy \\
&\quad = G_h(\mathbf{x}, \mathbf{z}) \int_{\Omega_z} [\nabla_h \cdot (\widehat{\epsilon}(\mathbf{y}) \nabla_h \widetilde{G}(\mathbf{y}, \mathbf{p})) - \nabla \cdot (\epsilon(\mathbf{y}) \nabla \widetilde{G}(\mathbf{y}, \mathbf{p}))]\, dy \\
&\quad = G_h(\mathbf{x}, \mathbf{z}) \oint_{S_\mathbf{z}} (\epsilon(\mathbf{s}) \nabla_h \widetilde{G}(\mathbf{s}, \mathbf{p}) - \epsilon(\mathbf{s}) \nabla \widetilde{G}(\mathbf{s}, \mathbf{p})) \cdot \vec{n}_z\, ds \\
&\quad + G_h(\mathbf{x}, \mathbf{z}) \sum_i \oint_{S(\mathbf{z}, \mathbf{z}_i)} (\widehat{\epsilon}(\mathbf{s}) \nabla_h \widetilde{G}(\mathbf{s}, \mathbf{p}) - \epsilon(\mathbf{s}) \nabla \widetilde{G}(\mathbf{s}, \mathbf{p})) \cdot \vec{n}_z\, ds.
\end{aligned} \tag{71}$$

Here, $S(\mathbf{z}, \mathbf{z}_i)$ denotes the cell face shared by the two cells Ω_z and Ω_{z_i}, $S_{\mathbf{z}}$ the set of cell faces shared by the boundaries of $b(A)$ and Ω_z (see Fig. 8), $\vec{n}_z$ the outward normal vectors on the boundary of Ω_z. Note that $\widehat{\epsilon} = \epsilon$ holds on the boundary of $b(A)$.

We estimate the two boundary integrals in (71) separately. From the definition of $b(A)$ in (38), it is seen that (15) holds on its boundary. Hence, we obtain the following upper bound of the former integral

$$\left| G_h(\mathbf{x}, \mathbf{z}) \oint_{S_{\mathbf{z}}} (\epsilon(\mathbf{s}) \nabla_h \widetilde{G}(\mathbf{s}, \mathbf{p}) - \epsilon(\mathbf{s}) \nabla \widetilde{G}(\mathbf{s}, \mathbf{p})) \cdot \vec{n}_z \, ds \right|$$

$$\leq c \frac{|S_{\mathbf{z}}| {h_0}^2}{|\mathbf{z} - \mathbf{x}||\mathbf{z} - \mathbf{p}|^4}. \tag{72}$$

with $|S_{\mathbf{z}}|$ the surface area of $S_{\mathbf{z}}$.

For the latter integral, we have to exploit the cancellation with the integrals from adjacent cells Ω_{z_i}. Let $\mathbf{w}$ be one of the adjacent grid points $\{\mathbf{z}_i\}$. Then, we find the following estimate from (14).

$$\begin{aligned}
&\left| G_h(\mathbf{x}, \mathbf{z}) \oint_{S(\mathbf{z},\mathbf{w})} (\widehat{\epsilon}(\mathbf{s}) \nabla_h \widetilde{G}(\mathbf{s}, \mathbf{p}) - \epsilon(\mathbf{s}) \nabla \widetilde{G}(\mathbf{s}, \mathbf{p})) \cdot \vec{n}_z \, ds \right. \\
&\quad \left. + G_h(\mathbf{x}, \mathbf{w}) \oint_{S(\mathbf{z},\mathbf{w})} (\widehat{\epsilon}(\mathbf{s}) \nabla_h \widetilde{G}(\mathbf{s}, \mathbf{p}) - \epsilon(\mathbf{s}) \nabla \widetilde{G}(\mathbf{s}, \mathbf{p})) \cdot \vec{n}_w \, ds \right| \\
&= \left| (G_h(\mathbf{x}, \mathbf{z}) - G_h(\mathbf{x}, \mathbf{w})) \oint_{S(\mathbf{z},\mathbf{w})} (\widehat{\epsilon}(\mathbf{s}) \nabla_h \widetilde{G}(\mathbf{s}, \mathbf{p}) \right. \\
&\quad \left. - \epsilon(\mathbf{s}) \nabla \widetilde{G}(\mathbf{s}, \mathbf{p})) \cdot \vec{n}_z \, ds \right| \\
&\leq c \frac{h_0}{|\mathbf{z} - \mathbf{x}|^2} \frac{{h_0}^3}{|\mathbf{z} - \mathbf{p}|^3} \leq c \frac{|\Omega_z| h_0}{|\mathbf{z} - \mathbf{x}|^2 |\mathbf{z} - \mathbf{p}|^3}.
\end{aligned} \tag{73}$$

From these estimates, finally we obtain the following upper bound for $|e_3|$

$$\begin{aligned}
|e_3(\mathbf{x}, \mathbf{p})| &= \left| \sum_{\mathbf{z} \in b(A)} \int_{\Omega_z} G_h(\mathbf{x}, \mathbf{y}) \nabla_h \cdot (\widehat{\epsilon}(\mathbf{y}) \nabla_h \widetilde{G}(\mathbf{y}, \mathbf{p})) \, dy \right| \\
&\leq c S^2(\partial A, \mathbf{p}) {h_0}^2 \left(\frac{1}{a_x {a_p}^2} + \frac{1}{{a_x}^2 a_p} \right)
\end{aligned}$$

Similarly, we also obtain (69). □

Remark. If we do not take the weighted harmonic average from (13) to determine $\widehat{\epsilon}(\mathbf{s})$, the truncation error at the discontinuity degrades. In that case, we can achieve only first order ($O(h_0)$) accuracy.

3.3. Error estimate of the solvation energy

The main interest in this section is how the accuracy of the solvation energy is related to the following quantities,

- The charge distribution of $\sum_i q_i \delta_{\mathbf{p}_i}$ in A.
- The grid extension rate α.
- The size of the finest grid D_0. In other words,

$$w := \mathrm{d}(A, \partial D_0). \tag{74}$$

Theorem 3.3. *From the results in Sect. 3.2, it follows that for a second order accurate solution of the solvation energy W_S the following three conditions must be fulfilled.*

- **Condition 1** *:* α must be at least $2^{2/3} \approx 1.587$.
- **Condition 2** *:* It is sufficient to choose w comparable to $\max_{i,j}\{|\mathbf{p}_i - \mathbf{p}_j|\}$.
- **Condition 3** *:* It is sufficient to choose w comparable to $\max_i\{a_{p_i} = d(\partial A, \mathbf{p}_i)\}$.

In the following, we explain how these conditions are induced.

Proof. First, we split the solvation energy into simpler terms. Let G_ϵ and G_{ϵ_0} be the Green functions of the diffusion operators $-\nabla\cdot(\epsilon\nabla\cdot)$ and $-\epsilon_0\nabla^2$, respectively. Then, the solutions of (1) and (5) are described as follows

$$\psi_\epsilon(\mathbf{x}) = \sum_i q_i G_\epsilon(\mathbf{x}, \mathbf{p}_i), \tag{75}$$

$$\psi_{\epsilon_0}(\mathbf{x}) = \sum_i q_i G_{\epsilon_0}(\mathbf{x}, \mathbf{p_i}). \tag{76}$$

Hence, the solvation energy in (4) is represented by

$$W_S = \frac{1}{2}\sum_{i,j} q_i q_j (G_\epsilon(\mathbf{p}_i, \mathbf{p}_j) - G_{\epsilon_0}(\mathbf{p}_i, \mathbf{p}_j)). \tag{77}$$

Although $G_\epsilon(\mathbf{p}_i, \mathbf{p}_i)$ and $G_{\epsilon_0}(\mathbf{p}_i, \mathbf{p}_i)$ are infinite, their difference is well-defined under the limit :

$$G_\epsilon(\mathbf{p}_i, \mathbf{p}_i) - G_{\epsilon_0}(\mathbf{p}_i, \mathbf{p}_i) := \lim_{\mathbf{x}\to\mathbf{p_i}} (G_\epsilon(\mathbf{x}, \mathbf{p}_i) - G_{\epsilon_0}(\mathbf{x}, \mathbf{p}_i)).$$

Hence, the error for W_S can be estimated by estimating the error of

$$G_\epsilon(\mathbf{p}_i, \mathbf{p}_j) - G_{\epsilon_0}(\mathbf{p}_i, \mathbf{p}_j) \tag{78}$$

for $i = j$ and $i \neq j$. For simplicity, we assume that all points $\{\mathbf{p}_i\}$ are just grid points. With (16), the estimates in this section are also valid for more

general cases.
The error for (78) with $i \neq j$ can be estimated by the error indicators $e_\epsilon(\mathbf{p}_i, \mathbf{p}_j)$ and $e_{\epsilon_0}(\mathbf{p}_i, \mathbf{p}_j)$ defined in (48) for the diffusion operators $-\nabla \cdot (\epsilon \nabla \cdot)$ and $-\epsilon_0 \nabla^2$, respectively.

From estimates (51) and (53) in Theorem 3.1, we obtain

$$|e_1(\mathbf{p}_i, \mathbf{p}_j)| \leq c \frac{\alpha^3 - 1}{1 - 2^2/\alpha^3} \left(\frac{|\mathbf{p}_i - \mathbf{p}_j|}{w} + 1 \right)^6 \frac{{h_0}^2}{|\mathbf{p}_i - \mathbf{p}_j|^3}, \tag{79}$$

$$|e_2(\mathbf{p}_i, \mathbf{p}_j)| \leq c \frac{1}{1 - 2^2/\alpha^3} \left(\frac{|\mathbf{p}_i - \mathbf{p}_j|}{w} + 1 \right)^5 \frac{{h_0}^2}{|\mathbf{p}_i - \mathbf{p}_j|^3}, \tag{80}$$

for $e = e_\epsilon$ and $e = e_{\epsilon_0}$. Hence, we find that Condition 1 and 2 are required to bound this error term.

The error for (78) with $i = j$ can be estimated by the following formula obtained from Green's identity.

$$\begin{aligned} G_\epsilon(\mathbf{x}, \mathbf{y}) - G_{\epsilon_0}(\mathbf{x}, \mathbf{y}) = \epsilon_0 \oint_{\partial\Omega} [\nabla (G_\epsilon(\mathbf{x}, \mathbf{s}) - G_{\epsilon_0}(\mathbf{x}, \mathbf{s})) G_{\epsilon_0}(\mathbf{s}, \mathbf{y}) \\ -(G_\epsilon(\mathbf{x}, \mathbf{s}) - G_{\epsilon_0}(\mathbf{x}, \mathbf{s})) \nabla G_{\epsilon_0}(\mathbf{s}, \mathbf{y})] \cdot \vec{n} \, ds \end{aligned}$$

$\forall\, \mathbf{x}, \mathbf{y} \in \Omega (\subset A)$. In particular, by substituting $\mathbf{p}_i$ for $\mathbf{x}$ and $\mathbf{y}$, we obtain

$$\begin{aligned} G_\epsilon(\mathbf{p}_i, \mathbf{p}_i) - G_{\epsilon_0}(\mathbf{p}_i, \mathbf{p}_i) = \epsilon_0 \oint_{\partial\Omega} [\nabla (G_\epsilon(\mathbf{p}_i, \mathbf{s}) \\ -G_{\epsilon_0}(\mathbf{p}_i, \mathbf{s})) G_{\epsilon_0}(\mathbf{s}, \mathbf{p}_i) - (G_\epsilon(\mathbf{p}_i, \mathbf{s}) - G_{\epsilon_0}(\mathbf{p}_i, \mathbf{s})) \nabla G_{\epsilon_0}(\mathbf{s}, \mathbf{p}_i)] \cdot \vec{n} \, ds. \end{aligned} \tag{81}$$

The above equation indicates that the error for $G_\epsilon(\mathbf{p}_i, \mathbf{p}_i) - G_{\epsilon_0}(\mathbf{p}_i, \mathbf{p}_i)$ can be estimated by the errors of $G_\epsilon(\mathbf{p}_i, \mathbf{s})$, $\nabla G_\epsilon(\mathbf{p}_i, \mathbf{s})$,etc for $\mathbf{s} \in \partial\Omega$. By choosing $\Omega = D_{a_{p_i}/2}(\mathbf{p}_i)$ for Ω in (81) and by applying the estimates from Theorem 3.1 and 3.2, we find that Condition 1 and 3 are required to bound this error term. □

4. Numerical experiments

In this section, we perform several numerical experiments with a model problem, where

$$\begin{aligned} &\epsilon_0 = 1, \\ &\epsilon_1 = 80, \\ &A = \{\mathbf{x} \,:\, \|\mathbf{x}\| \leq 1\}, \end{aligned}$$

and a unit point charge is located at the origin. The analytical solution of this problem is:

$$\psi_\epsilon(\mathbf{x}) = \begin{cases} \frac{1}{4\pi\epsilon_0\|\mathbf{x}\|} + \frac{1}{4\pi}\left(\frac{1}{\epsilon_1} - \frac{1}{\epsilon_0}\right) & \text{if } \|\mathbf{x}\| \le 1 \\ \frac{1}{4\pi\epsilon_1\|\mathbf{x}\|} & \text{if } \|\mathbf{x}\| > 1 \end{cases} \tag{82}$$

In Sect. 3, we have analyzed the relations between the numerical solution error and the grid extension rate, the finest grid domain size, etc. We want to determine whether the error analysis in Sect. 3 fits the results for this simple test problem well.

With (82), the solvation energy W_S for this simple problem is given by

$$W_S = \frac{1}{8\pi}\left(\frac{1}{80} - 1\right) \approx -0.03929137... \tag{83}$$

First, we investigate the influence of the discretization of ϵ at the discontinuity on the accuracy of the solvation energy. We compare two discretization methods to determine $\widehat{\epsilon}$. One is the weighted harmonic average (WHA) defined in (13), the other is the standard harmonic average (SHA) of sampled ϵ-values on two adjacent grid points. For instance, between two grid points $\mathbf{x}$ and $\mathbf{x} + (h_0, 0, 0)$, the SHA is defined as

$$\widehat{\epsilon}(\mathbf{x} + (h_0/2, 0, 0)) := \frac{2\epsilon(\mathbf{x})\epsilon(\mathbf{x} + (h_0, 0, 0))}{\epsilon(\mathbf{x}) + \epsilon(\mathbf{x} + (h_0, 0, 0))}. \tag{84}$$

In this experiment, we apply the conservative interpolation and fix the following parameters.

$$\begin{aligned} D_0 &= [-2, 2]^3, \\ \alpha &= 1.7, \\ m &= \mathrm{int}(\log_\alpha 10^6). \end{aligned} \tag{85}$$

Here, m denotes the number of levels. (85) implies that m is chosen in such a way that the coarsest grid domain size is at least 10^6 times larger than the finest grid domain size. We have 26 grid levels in these calculations. On the boundary of the coarsest grid, a zero Dirichlet boundary value is imposed.

In Fig. 9 the errors for the solution difference : $\psi_\epsilon - \psi_{\epsilon_0}$ along the line $\{(x_1, 0, 0) \ : \ x_1 \ge 0.0\}$ with the WHA (a) and with the SHA (b) are presented. The errors are measured for three finest grid spacings $h_0 = 0.25,\ 0.125$ and 0.0625. For the WHA, it is difficult to confirm the $O(h^2)$ accuracy as analyzed in Sect. 3.2. However, the error near the origin is better than $O(h^2)$ in this example. On the other hand, it is obvious that the improvement of the error with the SHA is less than $O(h^2)$. In particular, we see that the error with the SHA for the grid spacing 0.0625 is even larger

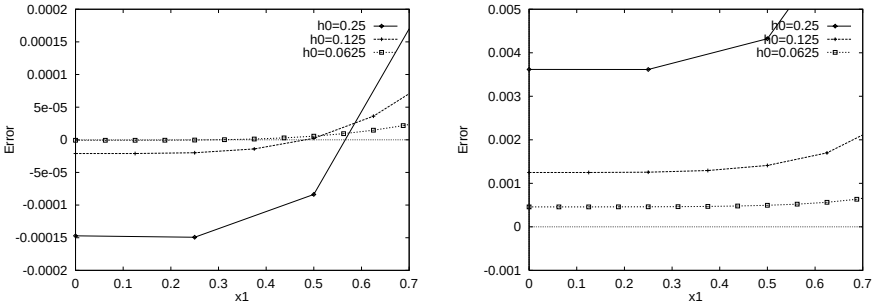

(a) with the WHA (b) with the SHA

Fig. 9a,b. The error for $\psi_\epsilon - \psi_{\epsilon_0}$ along a line $\{(x_1, 0, 0) \ : x_1 \geq 0\}$ with two discretizations of ϵ

than that with the WHA for the grid spacing 0.25. This result shows the importance of the discretization of the diffusion coefficient at the discontinuity to obtain an accurate solvation energy.

Next, we investigate the influence of the grid extension rate α on the accuracy of the numerical solvation energy. Here, $h_0 = 0.125$, D_0 and m are set as in the previous experiment and the weighted harmonic average is used to determine $\widehat{\epsilon}$. In Fig. 10 (a), the solvation energies computed with α from 1.4 to 1.8 are plotted for the conservative and cubic interpolation. For the conservative interpolation, the error curve is stable and close to the analytical solution for α larger than 1.7. The error does not diverge at $\alpha = 2^{2/3} \approx 1.587$ as indicated in Theorem 3.1. This can be explained from the fact that the grid extension rate is 2 in the far field as discussed in Sect. 2.1. For the cubic interpolation, we do not find a decrease of the error with an increase of α. This means that the error is not well defined by e in (48), because (47) does not hold due to the lack of the conservation at the interior boundaries.

In Fig. 10 (b), the solvation energies computed for various finest grid domain sizes are depicted. Here, α is set to 1.7 and the domain size changes from $[-1.25, 1.25]$ to $[-2.5, 2.5]$ in each direction. For the conservative interpolation, an accurate solvation energy is obtained for the external size w larger than 1, as indicated by Condition 3 in Sect. 3.3. With the cubic interpolation, the decrease of the solvation energy error with the increase of the size is again too small.

5. Conclusions and future work

In this paper, we have developed a theory to analyze the numerical errors in a potential problem with an unbounded domain, which arises in biomolecular simulations with a continuum solvent model. In the error analysis, under

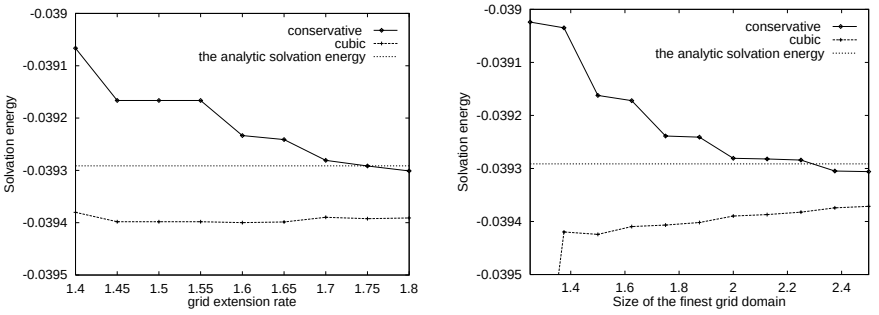

Fig. 10a,b. The solvation energies W_S computed for various grid extension rates in **a** and for various domain sizes in **b**. The broken horizontal line represents the analytic solvation energy

basic assumptions on the Green function, we have shown the proper ways to construct the composite grid around the solute molecule and to discretize the diffusion operator $-\nabla \cdot (\epsilon \nabla\ )$ around the ϵ-discontinuity.

Furthermore, we have proposed an interpolation technique on the interior boundaries of the composite grid based on a conservative discretization. The conservative interpolation is proposed for the general situation, where changing ϵ is also allowed at the interior boundaries. The experimental results confirm the error analysis theory developed in this paper, and it is found that the conservativeness of the discretization at the interior boundaries and a careful treatment of the ϵ-discontinuity are important issues to obtain accurate solutions.

References

1. R. E. Alcouffe, A. Brandt, J. E. Dendy, J. W. Painter, The multi–grid methods for the diffusion equation with strongly discontinuous coefficients, SIAM J. Sci. Stat. Comput. **2**, 430–454 (1981)
2. K. Aziz, A. Setari, Petroleum Reservoir simulation, Elsevier Appl. Sci. Publishers London (1979)
3. D. Bai, A. Brandt, Local mesh refinement multilevel techniques, SIAM J. Sci. Statist. Comput. **8**, 109–134 (1987)
4. A. Brandt, The Gauss Center research in multiscale scientific computing, Electr. Trans. on Num. Analysis **6,** 1–34 (1997)
5. M. J. Berger, A Jameson, Automatic adaptive grid refinement for the Euler Equations, AIAA Journal **23**, 561–568 (1985)
6. A. Brandt, Multigrid Techniques: 1984 Guide with Applications to Fluid Dynamics, GMD-Studie. **85**, GMD Sankt Augustin, Germany (1984)
7. C. Hirsch, Numerical computation of internal and external flows Vol. 1, J. Wiley, Chichester (1988)

8. D. Hoffmann, T. Washio, K. Gessler, J. Jacob, Tackling concrete problems in molecular biophysics using Monte Carlo and related methods: Glycosylation, Folding, Solvation, Monte Carlo Approach to Biopolymers and Protein, World Scientific, Singapore (1998)
9. M. J. Holst, Multilevel Methods for the Poisson-Boltzmann Equation, PhD thesis, University of Illinois, Urbana-Champaign, 1993
10. W. Hackbusch, Theorie und Numerik elliptischer Differentialgleichungen, B. G. Teubner, Stuttgart (1986)
11. J.Jost, Partielle Differentialgleichungen, Springer, Berlin (1998)
12. S. F. McCormick, Multilevel adaptive methods for partial differential equations, Frontiers in Applied Mathematics 6, SIAM, Philadelphia (1989)
13. F. M. Richards, Areas, volumes, packing and protein structure, Annu. Rev. Biophys. Bioeng., **6**, 151–176 (1977)
14. M. C. Thompson, J. H. Ferziger, An adaptive multigrid technique for the incompressible Navier-Stokes equations, J. Comput. Phys. **82**, 94–121 (1989)
15. P. Wesseling, An introduction to multigrid methods. John Wiley, Chicester (1992)